

## Article

# The Impacts of Urban Morphology on Urban Heat Islands in Housing Areas: The Case of Erzurum, Turkey

Cansu Güller \* and Süleyman Toy

Department of City and Regional Planning, Atatürk University, Erzurum 25240, Turkey;  
suleyman.toy@atauni.edu.tr

\* Correspondence: cansu.guller@atauni.edu.tr

**Abstract:** The growing importance of climate change underlines the need to comprehend Urban Heat Islands (UHI), particularly those influenced by urban morphology. As progress has been made in understanding the macroscale relationship between urban morphology and UHIs, the microscale effects are often overlooked. This study, conducted in the city of Erzurum in Turkey, delves into the complex relationship between urban morphology and UHI intensity in different housing areas with distinct microclimates, focusing particularly on street networks, building systems, and land use. Pearson correlation analysis was performed to investigate the relationships between morphological indicators and UHIs in different housing areas. Key findings include that (1) noticeable UHI effects were observed, especially in dense areas with high-rise buildings. (2) UHIs reveal a strong correlation with both 2D and 3D urban morphological indicators. A moderate-to-high Sky View Factor (SVF) tends to reduce UHIs, while an extremely high SVF aggravates UHIs. (3) Enhancing street network integration emerges as a more effective strategy for mitigating UHI effects in mid-rise buildings compared to other morphological factors. The Normalised Difference Built-Up Index (NDBI) and Normalised Difference Vegetation Index (NDVI) may not reliably indicate UHIs in housing areas with a predominantly rural character. Consequently, this article recommends that urban morphology optimisation for UHI mitigation should prioritise spatial and indicator specificity in urban design and spatial planning for cities. Future research endeavours should investigate the influence of morphological indicators on UHI dynamics in different seasons, including various remote sensing indicators related to morphological structure, to enrich our understanding of daily UHI fluctuations within urban morphology research.

**Keywords:** urban morphology; land surface temperature; sky view factor; space syntax; NDVI; NDBI



**Citation:** Güller, C.; Toy, S. The Impacts of Urban Morphology on Urban Heat Islands in Housing Areas: The Case of Erzurum, Turkey. *Sustainability* **2024**, *16*, 791. <https://doi.org/10.3390/su16020791>

Academic Editors: Amos Darko, K. Venkatachalam, Baojie He and Siliang Yang

Received: 2 December 2023

Revised: 14 January 2024

Accepted: 15 January 2024

Published: 17 January 2024



**Copyright:** © 2024 by the authors. Licensee MDPI, Basel, Switzerland. This article is an open access article distributed under the terms and conditions of the Creative Commons Attribution (CC BY) license (<https://creativecommons.org/licenses/by/4.0/>).

## 1. Introduction

In recent years, climate change-induced extreme weather events have emerged as pressing threats to communities [1,2]. The process of urbanisation significantly contributes to climate change by not only consuming energy and polluting the urban atmosphere but also by progressively transforming natural Earth surfaces into impermeable ones [3,4]. Urbanised surfaces continue to expand within cities, altering the urban structure and morphology to accommodate the rising human population [5–7]. This expansion, primarily the proliferation of built-up areas and impervious surfaces, significantly influences climate through the urban heat island (UHI) effect [8]. UHIs characterise the discernible temperature variance between microclimates within a city and its surrounding areas [9]. The expansion of cities has amplified the UHI effect, contributing to increased energy consumption, exacerbated pollution, and adverse effects on public health and well-being [10–12]. Thus, addressing this phenomenon promptly is crucial, necessitating a comprehensive understanding of the factors influencing UHIs to effectively mitigate their detrimental impacts.

Research has consistently highlighted various factors influencing UHIs, including climatic components, land surface characteristics, and notably, urban morphology [13,14].

While existing studies have primarily concentrated on the influence of climatic components and land surface characteristics on UHI formation, the role of urban morphology has emerged as a crucial factor driving UHI formation and expansion [15–17]. These morphological aspects significantly impact surface temperature [18–24], highlighting the importance of land use changes, impermeable surfaces, and vegetation cover in contributing to the UHI effect. However, while progress has been made in understanding the macro-scale relationship between urban morphology and UHIs, the microscale impact, particularly the influence of street network pattern, building form, and height, often remains overlooked in many cases.

The microscale impact of urban morphology on UHIs is noteworthy, altering the urban microclimate by reshaping the urban surface structure [25,26]. It has been observed that characteristics including street networks, building systems, and land use intensity at the micro-scale significantly affect UHIs [27]. Despite these insights, many analyses tend to focus on singular dimensions of spatial morphology, disregarding the comprehensive three-dimensional nature of urban form, which comprises street networks, building systems, and land use [28]. Building systems represent a 3D spatial morphology, while street networks and land use refer to a 2D spatial morphology.

Studies examining the relationship between the UHI effect and distinct urban morphology aspects often use the integration index as an indicator to analyse the street network [29–31]. This index, rooted in the Space Syntax Theory, identifies high-integration areas that foster consistent cooling effects compared to low-integration areas [32]. The impact of the building system, the second component of urban morphology, on UHIs is commonly assessed using the Sky View Factor (SVF) method. SVF, a 3D urban morphological indicator, significantly influences solar and terrestrial radiation, exhibiting a strong positive correlation with UHIs [33–35]. While areas with lower SVF experience slower heating due to building shadows, spaces with higher SVF heat faster due to increased solar radiation. The Normalised Difference Vegetation Index (NDVI) and the Normalised Difference Built-up Index (NDBI) constitute essential land use intensity indicators affecting micro-climate dynamics. Studies note a positive correlation between UHIs and NDBI and a negative correlation with NDVI [36–41].

The utilisation of geographic information systems (GIS) and correlation analysis has become a prevalent method for investigating the effect of morphological indicators on UHIs. While the majority of researchers have predominantly focused on examining the relationship between singular indicators of morphological components and UHIs, their consensus suggests a significant correlation [21–24,42]. Simultaneously, certain researchers have concentrated solely on the influence of building space [34,43,44], neglecting the mutual interaction between solar radiation and terrestrial radiation induced by enclosed building forms in diverse housing areas. This oversight has led to an insufficient explanatory power of morphology indicators for the UHI effect [27,45]. Consequently, there is a need for further exploration of the implications of these indicators in various housing areas. Understanding the intricate relationship between thermal conditions and morphological characteristics in housing areas is crucial for effective risk mitigation and the promotion of liveable spaces through sustainable urban planning strategies. Remote sensing-based land surface temperature (LST) obtained from satellite thermal bands serves as a pivotal tool for quantifying UHI intensity on broader scales [46–50].

This study aims to comprehensively investigate the effect of urban morphological components (street networks, building systems, and land use intensity indices) on UHIs in different housing areas characterised by distinct microclimate features. This study hypothesised that the impact of morphological indicators on UHIs varies in different housing areas. The study's focus on daytime summer conditions aligns with the evident health risks associated with rising temperatures during this period. This research aims to answer two key questions: (1) how do different morphological indicators impact UHI? (2) Are the effects of these indicators on UHI consistent across various housing areas?

## 2. Materials and Methods

### 2.1. Study Area

Three different housing areas with different morphological patterns were selected as the study area in Erzurum's city centre, situated in the north-eastern part of Turkey ( $39^{\circ}55' N$ ,  $41^{\circ}16' E$ ). Erzurum is one of the cities exposed to the largest amount solar radiation, depending on several factors (e.g., elevation; the actinometrical value is  $141 \text{ kcal/cm}^2$ ). The long-term (1991–2020) mean annual temperature is  $5.8^{\circ} C$ , the ever-recorded maximum temperature is  $36.5^{\circ} C$ , and the sunshine duration is 11 h. Three different housing areas were selected for the study, which were developed in different time periods and have different structural characteristics and morphological patterns. Study areas were determined as the housing areas of Dadaşket (northwest), Yenişehir-Yıldızkent (southwest), and Kayakyolu (southeast; Figure 1).

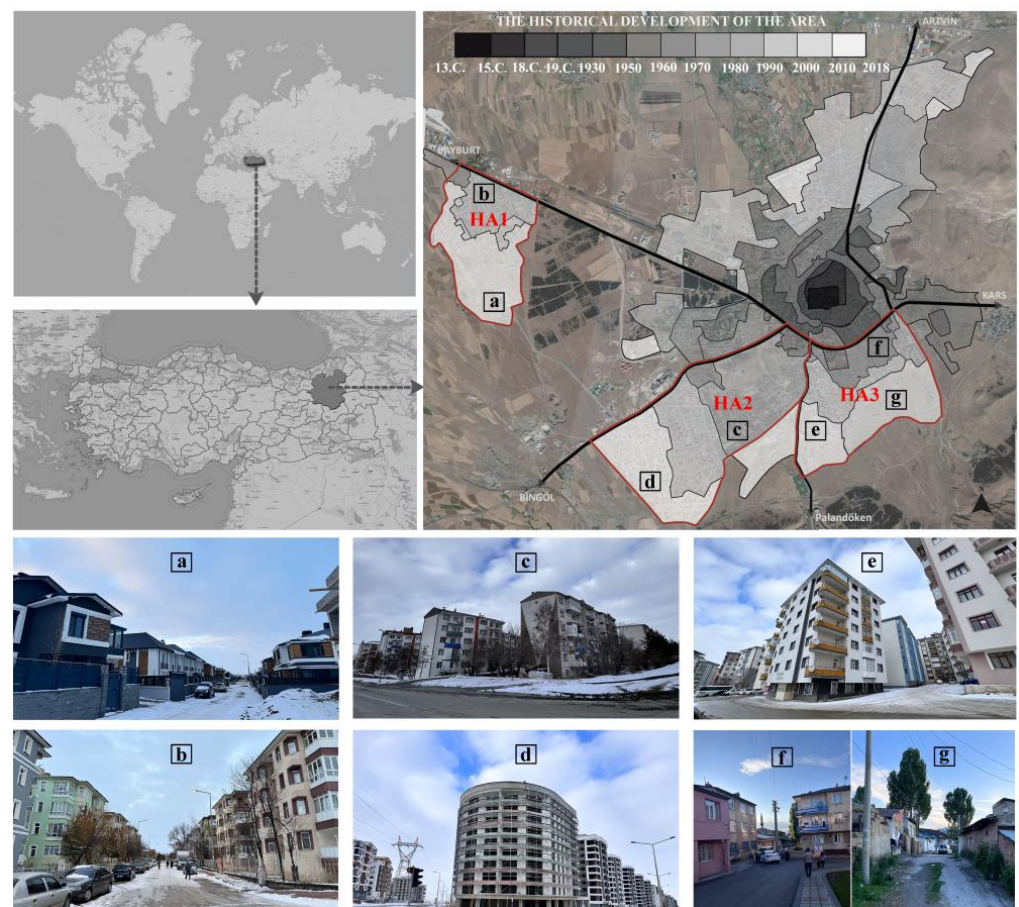


**Figure 1.** Chronological spatial development of the study area.

The range of housing patterns found in the study area highlights distinct characteristics in terms of building height, form, and arrangement, as well as street layout, resulting in a variety of urban canyon shapes. These distinct characteristics within the city of Erzurum provide an excellent context for examining how urban morphology influences thermal conditions.

The study was conducted in three housing areas that were developed under the Zeki Yapar Development Plan of 1967. Despite the development during the same planning periods, these areas have different morphological characteristics due to distinct urban development processes [51]. This different pattern was chosen as the study area because it provides an opportunity to compare the impact of three distinct urban morphologies on the UHI.

Dadaşkent housing area (HA1) was proposed as a satellite city for urban growth in the plan and has experienced rapid development since 1990. Over time, the storey heights of housing buildings have increased up to 5 storeys, with courtyard blocks being built in the southern part of the area since 2010. Notable characteristics of this area consist of a grid-like street structure composed of a main axis and streets branching off the main axis.

The Yenişehir and Yıldızkent housing areas (HA2) were constructed by cooperatives between 1980 and 1990 to address the slum problem experienced between 1970 and 1980. The development in the north of HA2 is characterised by mid-rise, linear block buildings. Throughout the planning, design, and implementation phases, the emphasis was on achieving a balance between open and closed spaces. The orientation of streets and avenues was determined based on the prevailing wind direction. However, since 2010, the area has become a major focal point for city development due to its increasing attractiveness. In the southern part of HA2, there has been a recent architectural trend towards high-rise buildings with point blocks, leading to a greater variety of housing building forms in the area.

The Kayakyolu housing area (HA3), located in the southeast of the city, has experienced spatial development at different times. The northern area of HA3 was mainly composed of low-rise buildings that were initially inhabited by individuals who migrated to the city during the 1960s. As the income levels of residents increased over time, these structures evolved into 3- to 4-storey buildings. The transportation infrastructure within this area developed in an unplanned manner, lacking a systematic design or organisation. Conversely, the southern part of the area underwent development after the introduction of the Zeki Yapar Plan. This plan led to the construction of high-rise apartment buildings that differed from the existing texture. It is important to note that although the development was carried out after the planned period, the road routes were implemented irregularly in practice. This unique texture combined unplanned low-rise buildings with a high rural character and planned high-rise buildings, creating a unique mixture of building forms and spatial arrangements in the surrounding area.

## 2.2. Time Period

The study period was determined to be July 2022 due to the prevalence of mostly clear skies during this month. Specifically, 15 July was chosen, as it exhibited a very low mean cloudiness rate of 0.05 octas. This date offered optimal image quality and was characterised by a monthly maximum temperature of 33 °C and a minimum temperature of 14 °C, according to data from the Erzurum Meteorological Administration.

## 2.3. Materials

NDBI, NDVI, and LST were calculated using remote sensing data from the Landsat 8 Operational Land Imager (OLI), provided by the USGS. The Landsat-8 OLI image, captured during the summer daytime (July 2022 at 07:56), constituted the dataset used.

Street network data for the integration (RN) analysis, which describes the degree of integration of a street with other streets in the city, were obtained from two main sources: Open Street Map (OSM) and the General Directorate of Highways database referred to as Atlas [52]. Leveraging these open-source platforms offers updated location data and inherent advantages.

Given the variable nature of the data from Atlas and OSM, the confidence in the information was cross verified using additional sources, including Google Maps, Google Streets, and Environmental System Research Institute (ESRI) Streets. To produce a full and detailed visualisation, all the fundamental maps were overlapped and integrated within the GIS environment. Ultimately, a cohesive and conclusive map was generated by integrating data from various sources.

Field surveys were conducted to identify housing areas and green spaces within each HA. Although the study area includes green spaces known for their cooling effect, it is important to mention that previous research has highlighted the cooling influence of a

24 ha green space extending up to distances of 200–250 m [53,54]. Therefore, to ensure accuracy, the cooling effect attributed to these green spaces was excluded from the analysis.

Building heights and forms were classified into eight categories, comprising irregular houses, detached houses, traditional Erzurum apartment houses, courtyard blocks, linear blocks, mid-rise apartments, high-rise apartments, and point blocks. Sky View images were captured at eight different control points, each of which represented a different building height and form, for the SVF analyses.

#### 2.4. Methods

The general methodology procedure is given in Figure 2.

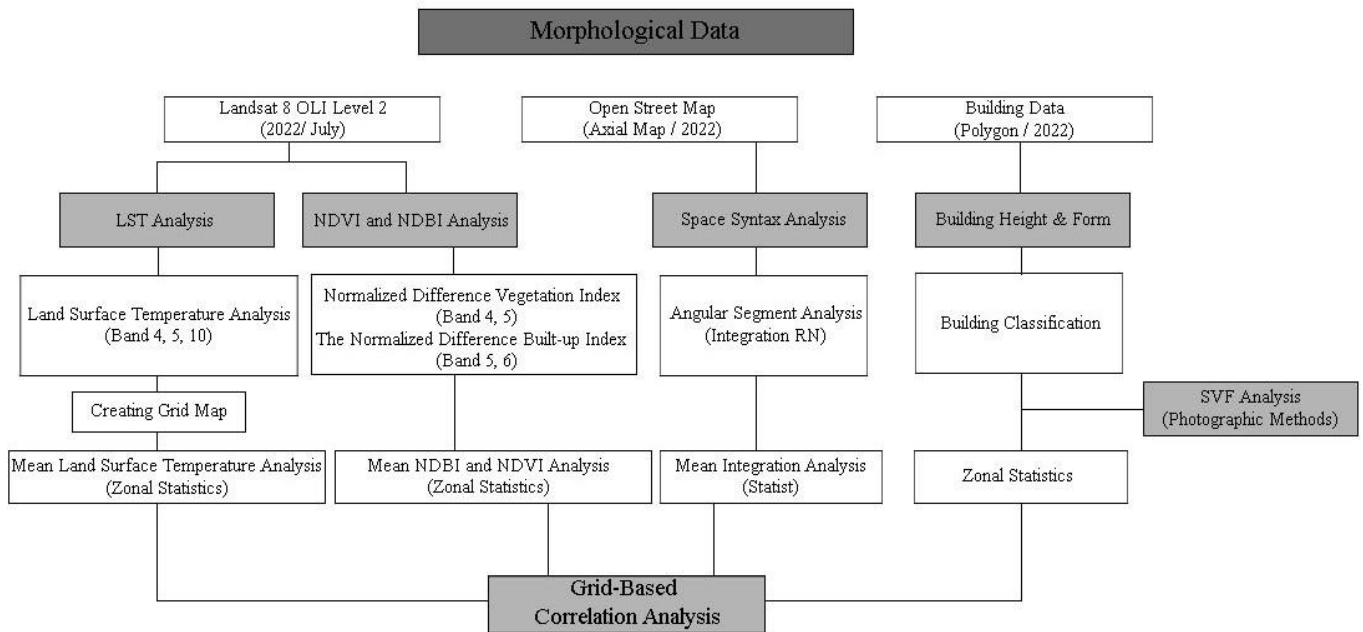


**Figure 2.** Flow chart of the method.

##### 2.4.1. Land Surface Temperature Analysis

Calculations of LST provide a prominent technique for illustrating the spatial distribution of the UHI phenomenon, which has been extensively studied in the literature [55,56]. The NDVI equation is crucial when calculating LST, particularly due to the well-known ability of urban green spaces to alleviate LST [57].

QGIS 3.12 software was used for the LST analysis, and the raster calculator tool was used to calculate LST from Landsat 8 OLI bands. Band 10 from the two thermal infrared sensors (TIRS) integrated into Landsat 8 was specifically chosen for its higher accuracy in LST calculations, as highlighted in the research by Yu et al. [58]. In order to determine LST, it is essential to first convert Band 10 digital number (DN) values into Top-of-Atmosphere (TOA) radiance using the following equation [55]:

$$\text{Top of Atmosphere (TOA)} = \text{ML} \times \text{Qcal} + \text{AL} \quad (1)$$

where Qcal denotes band 10, ML represents a band-specific multiplicative rescaling factor obtained from metadata, and AL stands for an additive rescaling factor.

After converting DN values to TOA radiance, the TIRS band data should be further transformed into brightness temperature (BT) using the thermal constants provided in the metadata. The calculation of BT from satellites involves deriving the absolute temperature (in Kelvin) from TOA data, typically employing the relationship depicted in Equation (2) [59].

$$\text{Brightness Temperature (BT)} = \frac{K2}{\ln\left(\frac{K1}{TOA} + 1\right)} - 273.15 \quad (2)$$

where BT is the at-satellite brightness temperature. K1 and K2 are the thermal constants of TIR band 10 from the metadata.

The calculation of NDVI is necessary for further determining proportional vegetation (Pv) and emissivity ( $\epsilon$ ). Band 4 and Band 5, representing the red and near-infrared bands of Landsat-8 OLI [60], were used in the NDVI equation as given by Equation (3). The LST is calculated by Equation (6) using BT, NDVI, and  $\epsilon$  by land use type.

$$\text{NDVI} = \frac{\text{Band5} - \text{Band4}}{\text{Band5} + \text{Band4}} \quad (3)$$

$$\text{The proportion of vegetation (Pv)} = \left[ \frac{\text{NDVI} - \text{NDVImin}}{(\text{NDVImax} - \text{NDVImin})} \right]^2 \quad (4)$$

$$\text{Emissivity } (\epsilon) = 0.004 \times \text{Pv} + 0.986 \quad (5)$$

$$\text{Land Surface Temperature (LST)} = \frac{\text{BT}}{1 + (0.00115 \times \frac{\text{BT}}{1.4388})} \times \text{Ln}(\epsilon) \quad (6)$$

where Pv provides an estimation of the area under each land cover type and is acquired from the NDVI of pure pixels. Emissivity is defined as a measure of absorptivity [61].

#### 2.4.2. Space Syntax Analysis

The Space Syntax analysis examines street networks to precisely define urban spaces by quantitatively computing morphological characteristics based on linkages shown in segment maps [62]. At the urban scale, axial lines represent street segments, and Space Syntax focuses on the topological dimension of the street network, specifically how axial lines interconnect [63]. The degree of integration assesses the extent to which the initial segment is integrated into the global system, with greater integration indicating a higher number of connections to the network [64].

The analysis of Space Syntax was conducted using the DepthmapX (version 0.8.0) software. Initially, an axial map of Erzurum city was generated in QGIS 3.12. Subsequently, the data underwent angular segment analysis within the DepthmapX software after being transformed into shapefile format.

Space Syntax is based on the four steps [65] illustrated in Figure 3:

- i. The street pattern (1) is transformed into an axial map (2), which is, albeit not precisely a graph, still a rudimentary representation.
- ii. The axial map (2) is transformed into a binary graph (3), referred to as a connectivity graph. This undirected graph consists of N nodes, the number of axial lines, and K links, representing intersections between pairs of axial lines.
- iii. Integration, a vital measure in Space Syntax, is determined through Equations (7) and (8). Within Space Syntax, the distance between two spaces is computed using a depth value [66]. In the computation of integration, Space Syntax typically calculates topological distance, which is defined as the minimum number of directional changes from each street segment to all others, commonly referred to as depth [65].

$$\text{MD}_i = \frac{\text{TD}_i}{n-1} = \frac{\sum_{j=1}^n d_{ij}}{n-1} \quad (7)$$

where,  $\text{MD}_i$  is the mean depth value of space  $i$ ,  $\text{TD}_i$  represents the total depth value of space  $i$ , and  $d_{ij}$  defines the shortest way from space  $i$  to  $j$ .

$$RRA_i = \frac{2(MD_i - 1)}{(n - 2) \times D_n} \quad (8)$$

$$D_n = \frac{2 \left( n \left( \frac{\log_2(n+2)}{3} - 1 \right) + 1 \right)}{(n-1) \times (n-2)}$$

where  $D_n$  is used for providing a standardised value for the integration measure, and  $RRA_i$  represents the RRA value for space  $i$ .

- iv. The integration of each node in the integration graph (3) is computed, and the colour-coded values are then mapped back onto the axial map (4), culminating in a final primitive-like colour-coded representation [65].

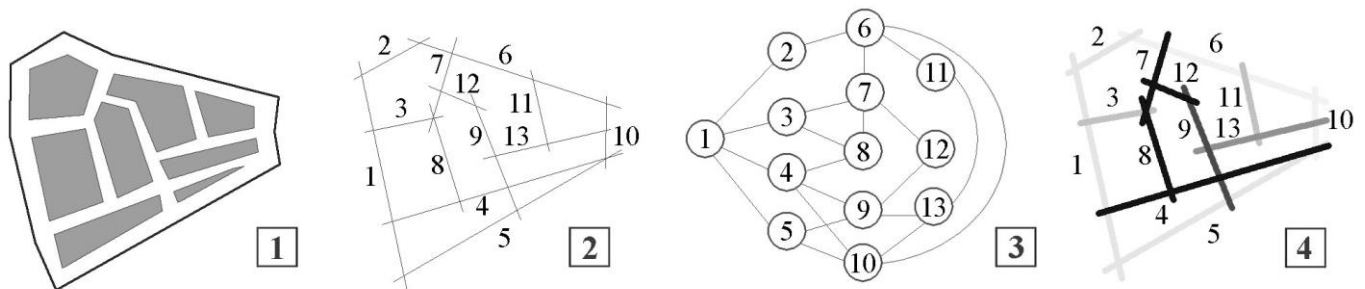


**Figure 3.** Diagram of the basic steps in the Space Syntax [65]. (1) street pattern, (2) axial map, (3) binary graph, (4) integration map.

#### 2.4.3. Sky View Factor Photographic Analysis

Optical and photographic techniques serve as means to ascertain the SVF [67]. Photographic methodology involves the use of a fisheye lens to capture urban canyon images [68,69]. Fisheye lenses intentionally distort image edges, providing a wide-angle view and a slightly curved perspective.

As there is no standardised height for capturing SVF images [70], images were taken in this study by positioning at the base of an urban canyon, lying in the middle of the street, and raising the hand vertically at eight points, representing diverse building heights and forms. The photos were taken during clear sky conditions in the summer.

Adobe Photoshop (version CS6) software was employed to calculate SVF values from these images [69,71]. The magic wand tool in Photoshop facilitated the selection of visible sky areas, automatically detecting open sky areas based on blue pixel values. Careful attention was paid to distinguish between blue sections of buildings and the actual sky during the automatic selection process.

This approach effectively identified SVF, even in images captured under tree canopies, by distinguishing the blue sky amidst branches and leaves. After accurately selecting the sky colour, the total count of all visible pixels in the fisheye lens image ( $\beta$ ) and the number of pixels representing the visible sky ( $\alpha$ ) were determined. Both pixel counts were recorded in Microsoft Excel, and SVF values were calculated using the  $\alpha/\beta$  equation following the methodology outlined in Debbage [71].

#### 2.4.4. NDBI and NDVI Analysis

The use of Landsat bands allows for the evaluation of land use intensity indices (NDVI and NDBI) using various methods [35,72–74]. Spectral index techniques rely on the electromagnetic spectrum's wavelength-related properties and the spectral behaviour of residential landscapes regarding absorption or reflection. In this context, built-up and bare lands tend to reflect more short-wave infrared radiation (SWIR) compared to near-infrared radiation (NIR). On the other hand, water bodies do not reflect in the infrared spectrum. Healthy green surfaces typically show higher reflectance in the NIR spectrum compared to the SWIR spectrum. These distinct bands within satellite images represent different

wavelengths of the electromagnetic spectrum, forming the basis for various spectral index methods and their respective formulas and calculation approaches [75].

NDVI stands out as one of the most widely used land use intensity indices for evaluating plant densities [76–79]. Healthy vegetation, due to its chlorophyll content, tends to strongly absorb blue and red spectra while reflecting the green spectrum, which is why healthy vegetation appears green. NDVI is computed using the high reflectance in NIR and the high absorption in the red spectrum, as outlined in Equation (9):

$$\text{NDVI} = \frac{\text{NIR} - \text{Red}}{(\text{NIR} + \text{Red})} \quad (9)$$

In Landsat 8 OLI data,  $\text{NDVI} = \frac{\text{Band 5} - \text{Band 4}}{\text{Band 5} + \text{Band 4}}$ .

Generally, NDVI values from  $-1$  to  $0$  represent bodies of water;  $-0.1$  to  $0.1$  barren rocks, sand, or snow;  $0.2$  to  $0.5$  bushes, pastures, or ageing crops; and  $0.6$  to  $1.0$  dense vegetation or tropical rainforest [75].

The NDBI is a valuable indicator used to measure built-up density [80,81]. It stands out among various land use classes due to its distinct spectral response. The formula for calculating NDBI is expressed as Equation (10).

$$\text{NDBI} = \frac{\text{SWIR} - \text{NIR}}{\text{SWIR} + \text{NIR}} \quad (10)$$

For Landsat 8 data,  $\text{NDBI} = \frac{\text{Band 6} - \text{Band 5}}{\text{Band 6} + \text{Band 5}}$ .

The NDBI value lies between  $-1$  and  $1$ . Larger values represent build-up areas. The NDBI value for vegetation is lower.

In this research, calculations were conducted using Landsat 8 OLI satellite image bands. For the analysis of NDVI and NDBI, QGIS 3.12 software was employed, utilising the raster calculator tool to derive values from the Landsat 8 OLI bands.

#### 2.4.5. Statistical Analysis among Integration (Space Syntax), SVF, NDVI, NDBI, LST

For the purpose of statistical analysis, the study area was systematically divided into uniformly spaced grids of  $500$  m, aligning with the methodology employed in prior studies [82–84]. The utilisation of  $500$  m grids also facilitates the assessment of street network integration and the monitoring of variations in housing forms. This grid segmentation was executed using the fishnet tool integrated into QGIS 3.12 software. A total of  $55$  grids were delineated in HA1,  $70$  in HA2, and  $53$  in HA3, and values for LST, NDBI, NDVI, integration, and SVF were determined for each grid cell.

IBM SPSS Statistics 22 software was used to analyse the effect of morphological components on LST. The initial data collected from the three different HAs was subjected to a normality test (Kolmogorov–Smirnov). One-way ANOVA analysis in SPSS was used to confirm differences in LST trends between HAs, followed by Duncan’s multiple comparison test to assess mean differences between subclasses.

LISA analysis using the Global Moran Index was performed to determine the distribution pattern of LST within the three HAs. This method provided an indication of whether LST values were clustered or dispersed across these areas. The high-high and low-low grid designations denoted spatial clusters, indicating areas where both the grid itself and its surrounding grids had either high or low LST values. Conversely, the high-low and low-high designations signified spatial outliers, representing grids with contrasting LST values compared to their adjacent areas [85]. The colourless dots on the analysis map indicated grids without statistically significant clustering or outlier characteristics relative to their surroundings.

Pearson correlation analyses were performed to determine the significance and nature of the relationship between LST and morphological parameters (integration, SVF, NDVI, and NDBI) within the three different HAs.

### 3. Results

#### 3.1. Results of Land Surface Temperature Analysis

The study areas demonstrated a spatial distribution of LST ranging from 41.86 °C to 68.66 °C. It is worth highlighting that the highest LST value was recorded in HA2, which is characterised by high-rise, point block buildings. In contrast, mid-rise and low-rise buildings in HA1 and HA3 had relatively lower LST values (Figure 4).

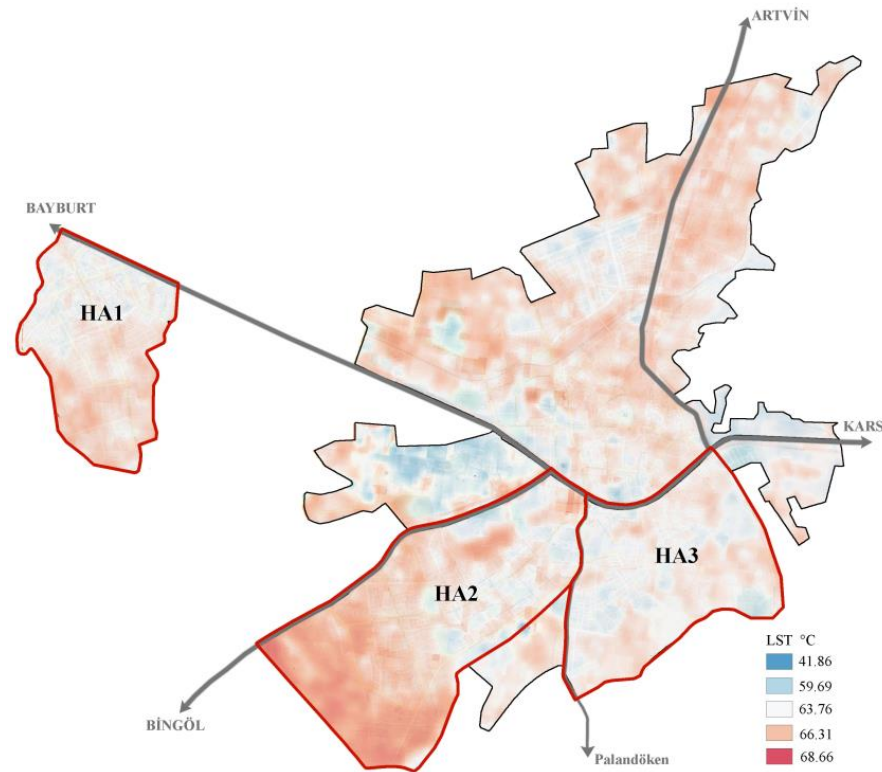


**Figure 4.** Spatial distribution of LST in the study areas.

Analysis of LST in the different HAs revealed that HA2 had the highest average LST at 64.96 °C, placing it in first place. This was closely followed by HA1 in second with a 64.44 °C average LST. Meanwhile, HA3 had the lowest LST of 63.97 °C, resulting in third place (Table 1). This significant difference in LST values emphasises the thermal differences between the different HAs.

**Table 1.** The Duncan's Multiple Comparison Test results of LST values for the HAs in the study area.

HA1 Mean LST Value	HA2 Mean LST Value	HA3 Mean LST Value	<i>p</i> Value
64.44 <sup>a</sup>	64.96 <sup>b</sup>	63.97 <sup>c</sup>	<i>p</i> = 0.000

<sup>a, b, c</sup> The means shown in different lowercase letters between the groups (on the line) are statistically significant. *p* < 0.05: Statistically significant.

The LISA analysis findings revealed patterns of LST clustering in both HA1 and HA2. However, no significant clusters or outliers were detected in HA3. HA1, the northern sector characterised by mid-rise apartments, displayed clusters with low-low values. On the other hand, the southern region, dominated by detached houses, exhibited clusters with high-high values. Noteworthy is that the southern part of HA2, experiencing rapid development with high-rise point block buildings, demonstrated high-high clusters, suggesting an elevation in LST. Conversely, the northern area of HA2 exhibited low-low clusters (Figure 5).

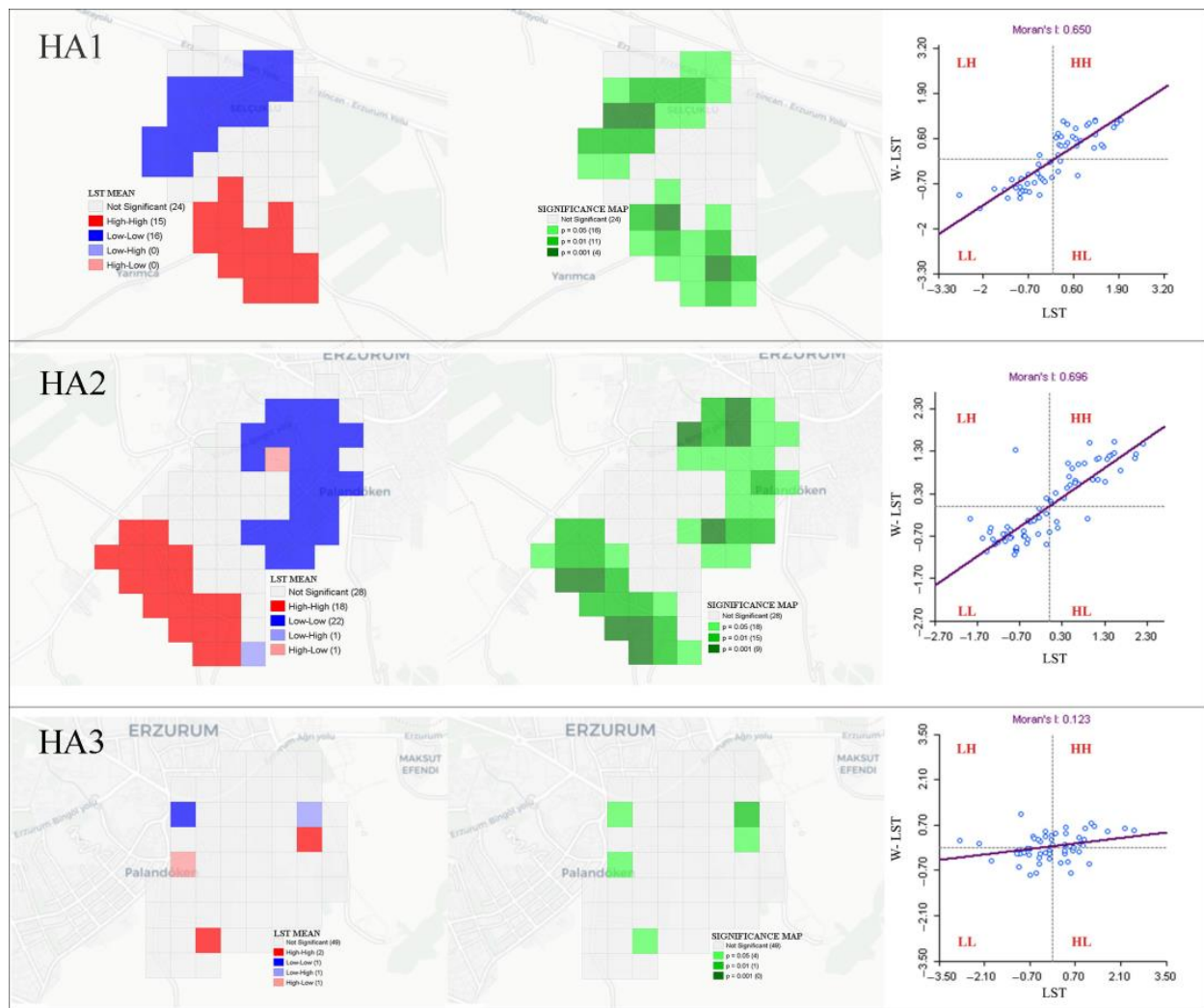


**Figure 5.** Local indicators of spatial association analysis.

### 3.2. Results of Space Syntax Analysis

Figure 6 illustrates the integration index of Erzurum's street network, representing a spectrum of integration values in different shades from light to dark, depicting a range from low to high integration. Notably, the main axis indicated a higher level of integration, which gradually decreased towards the periphery of the city. The three HAs revealed differences in integration indices. HA1 presented integrated areas in the northern and southern regions, with integration decreasing towards the periphery. A noteworthy feature of HA2 was the high rate of integration, which could be attributed to the grid street network design aligned with the prevailing wind direction. The southern area of HA2, which is experiencing rapid urban expansion, displayed amplified integration as a result of planned boulevards. Conversely, in HA3, there was a higher level of integration in the unplanned northern sectors, with a corresponding decline as progress was made towards the southern areas.

### 3.3. Results of NDVI and NDBI Analysis

Tables 2 and 3 provide statistical insights into NDBI and NDVI values in the three HAs. It was evident from these tables that HA2 exhibited a higher NDBI, indicating more intense built-up areas compared to the others, along with a lower proportion of green spaces. Conversely, HA1, predominantly characterised by detached houses, displayed lower built-up areas and higher green spaces. The maps depicting the NDBI and NDVI distributions (Figure 7) clearly illustrated the disparities in index values among the HAs.

The NDVI value in the public zone (empty area) in the northwest of HA2 appeared higher due to ongoing construction activities for a new housing area. However, this particular zone was excluded from the study, focusing solely on the data from existing housing areas.

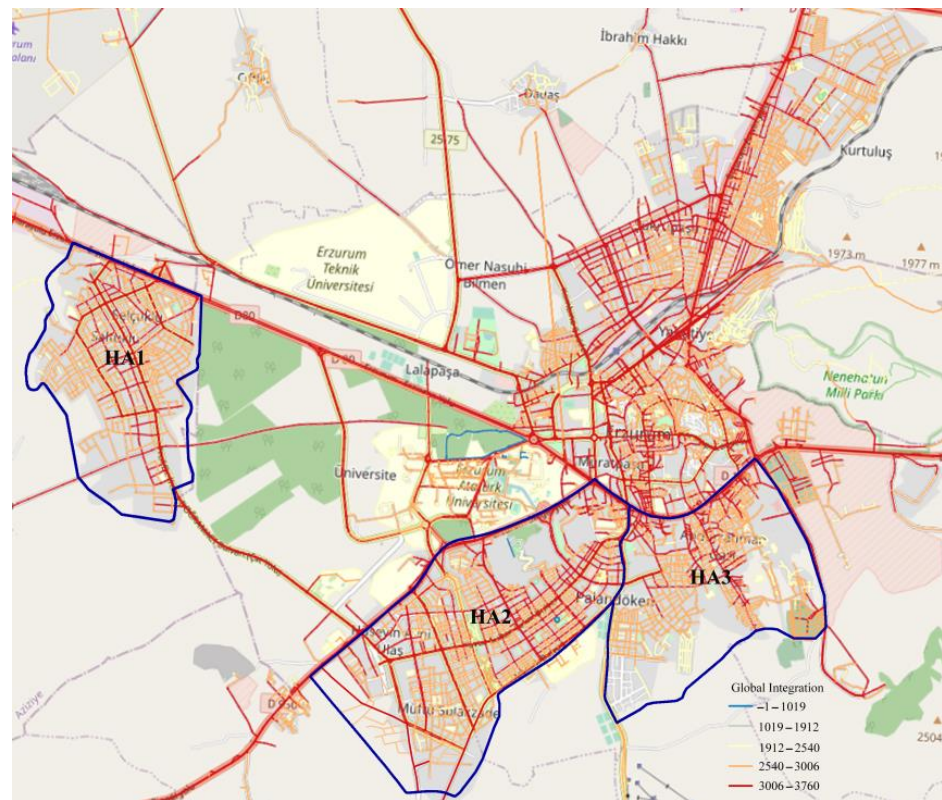


Figure 6. The integration index of axial lines.

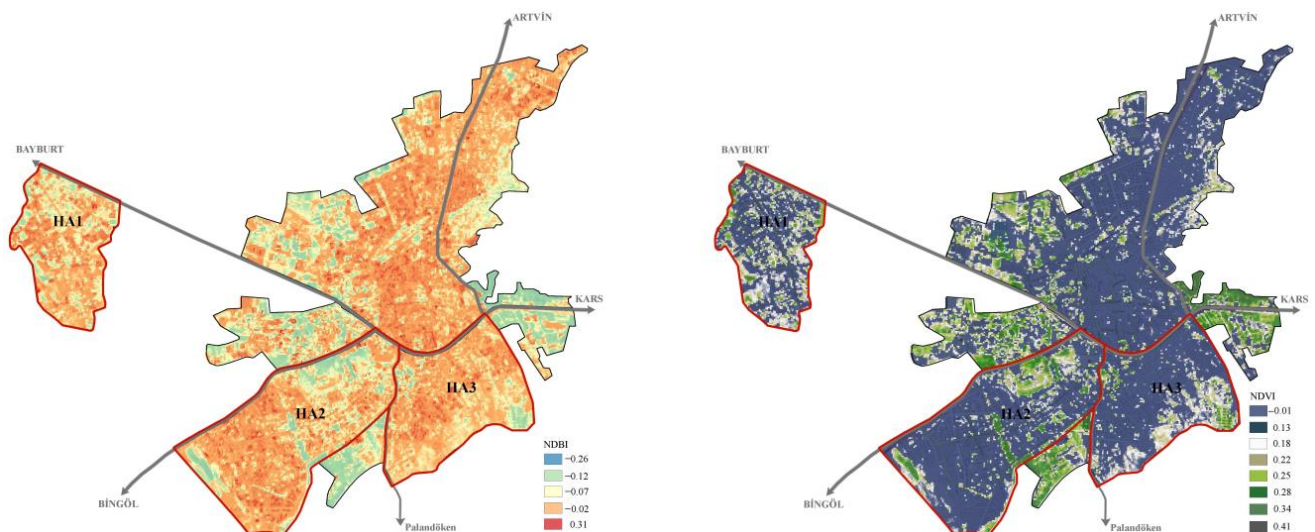


Figure 7. NDBI and NDVI maps.

Table 2. Statistical data of the NDBI for HAs.

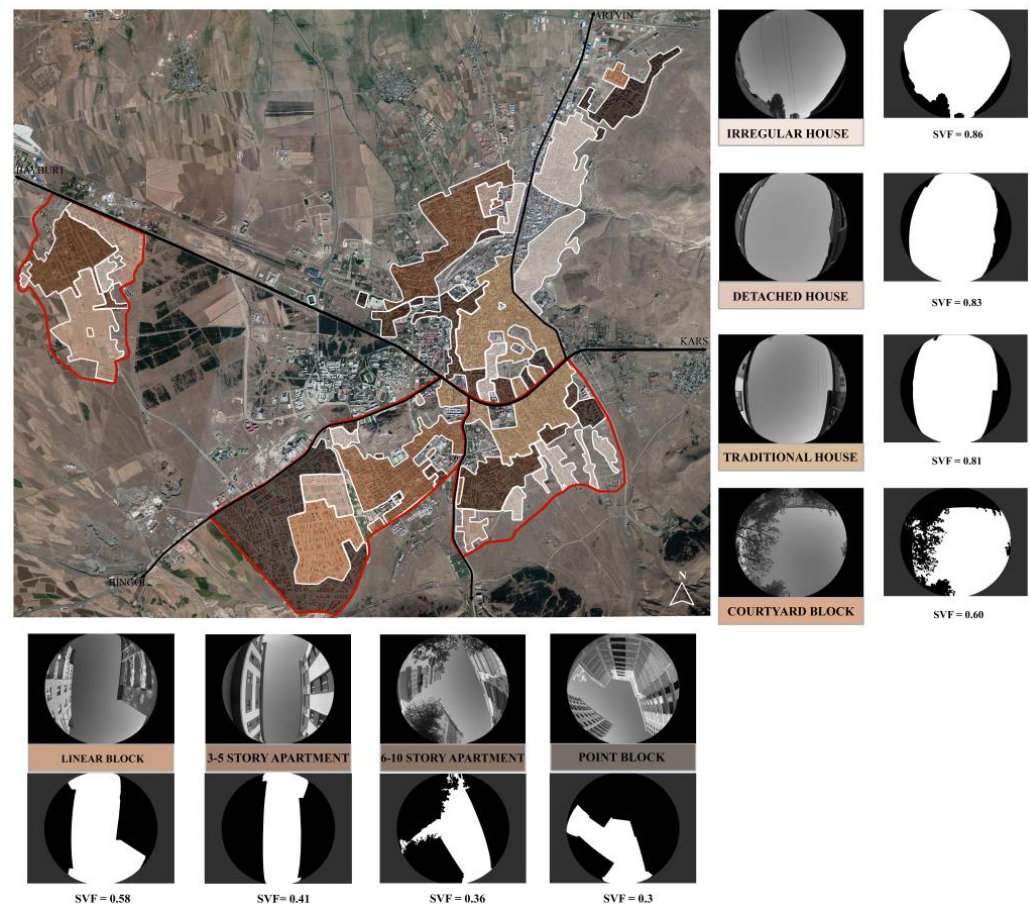
Area	Minimum	Maximum	Mean	Standard Deviation
HA1	−0.26	0.31	0.02	0.06
HA2	−0.24	0.28	0.03	0.06
HA3	−0.22	0.21	0.03	0.05

**Table 3.** Statistical data of the NDVI for HAs.

Area	Minimum	Maximum	Mean	Standard Deviation
HA1	0.00	0.41	0.17	0.06
HA2	−0.01	0.41	0.13	0.07
HA3	−0.01	0.39	0.14	0.06

### 3.4. Results of Sky View Factor Photographic Analysis

Different morphological characteristics were observed in the three HAs based on the building heights and forms. HA1's northern area was characterised by mid-rise apartments, while the southern part was comprised of detached houses. HA2's northern section was dominated by mid-rise building blocks, featuring linear blocks and courtyard blocks. The southern part of HA2 demonstrated an urban configuration dominated by high-rise point block buildings. HA3 exhibited a diverse urban pattern, including low-rise, irregular housing with high rural character in the south and high-rise apartments in the southwest. SVF analyses were conducted using sky images captured from eight distinct points, each representing the various housing heights and forms mentioned above. Figure 8 demonstrates the results obtained from the SVF analysis.

**Figure 8.** SVF analysis of different housing typologies.

The findings indicated that high-rise apartment buildings produced lower SVF values, whereas low-rise buildings demonstrated higher SVF values. Moreover, courtyard and linear blocks generally resulted in higher SVF values since courtyard blocks had shared spaces between the buildings and linear blocks had spaces on two sides. Noteworthy, an examination of various high-rise point block buildings and typical high-rise apartments revealed distinctive patterns in SVF. This observation underscores the influence of both

housing forms and heights on SVF, indicating a nuanced relationship that contributes to the variability in SVF patterns.

### 3.5. Results of Correlation Analysis among Integration (Space Syntax), SVF, NDVI, NDBI and LST

This study examined correlations between LST and morphological indicators using 500 m gridded averages within three different HAs. The Pearson correlation results highlighted variations in the morphological characteristics of these HAs. The findings indicated that LST levels tended to increase with higher NDBI values and decrease with higher NDVI values. Notably, HA1 and HA2 demonstrated a strong positive correlation between NDBI and LST, while NDVI had a significant negative effect on LST in both HA1 and HA2. In contrast, no significant correlation was observed between these land use intensity indices (NDBI and NDVI) and LST in HA3.

The HA3 was noteworthy for its mixed building form, which consisted of unplanned low-rise buildings and planned high-rise apartment buildings. This exceptional composition resulted in variations in LST that could not be attributed entirely to increases in NDBI and NDVI. Therefore, the SVF was an important factor to understand for LST variation. The various types of buildings, with their different heights and forms, significantly affected SVF, especially in the HA3. Thus, it was determined that SVF demonstrated a positive correlation with LST in HA3 (Table 4).

**Table 4.** Results of the correlation analyses between SVF and LST in HAs.

	LST (HA1)	LST (HA2)	LST (HA3)
SVF (HA1)	0.597 **		
SVF (HA2)		−0.698 **	
SVF (HA3)			0.416 *

\* Correlation is significant at the 0.05 level (two-tailed). \*\* Correlation is significant at the 0.01 level (two-tailed).

However, a contrasting scenario was observed in HA2, where the prevalence of high-rise, point block buildings resulted in remarkably low SVF values. Despite the reduced solar radiation reception due to extremely low SVF, these areas experienced high levels of terrestrial radiation. This complex juxtaposition led to an elevation in LST. The synergy between the extremely low SVF and diminished NDVI values in HA2 contributed to increased LST. Indeed, the absence of NDVI's cooling effect and the dominance of increased terrestrial radiation, despite notably low SVF levels, likely contributed to this scenario.

The integration index exhibited a strong correlation in different HAs, making it a key indicator for explaining LST (Tables 5–7). Similar to the SVF, this index indicated a correlation with reduced LST values in both detached and low-rise buildings. The correlation was possibly due to increased shading in integrated areas. In HA1 and HA3, a notably strong negative correlation was found between the integration index and LST. Contrary to expectations, HA2 exhibited a remarkable reversal in the relationship between the integration index and LST. This remarkable shift challenged conventional assumptions, offering a new perspective on understanding the intricate dynamics between high-rise buildings and LST.

**Table 5.** Results of the correlation analyses between multiple urban morphological indicators in HA1.

	LST	INTEGRATION	SVF	NDBI	NDVI
LST	1				
INTEGRATION	−0.607 **	1			
SVF	0.597 **	−0.280	1		
NDBI	0.400 **	−0.267	0.039	1	
NDVI	−0.378 **	−0.062	0.002	−0.936 **	1

\*\* Correlation is significant at the 0.01 level (two-tailed).

**Table 6.** Results of the correlation analyses between multiple urban morphological indicators in HA2.

	LST	INTEGRATION	SVF	NDBI	NDVI
LST	1				
INTEGRATION	0.424 **	1			
SVF	−0.698 **	−0.225	1		
NDBI	0.520 **	0.421 **	−0.423 **	1	
NDVI	−0.528 **	−0.513 **	0.395 **	−0.933 **	1

\*\* Correlation is significant at the 0.01 level (two-tailed).

**Table 7.** Results of the correlation analyses between multiple urban morphological indicators in HA3.

	LST	INTEGRATION	SVF	NDBI	NDVI
LST	1				
INTEGRATION	−0.453 **	1			
SVF	0.416 *	−0.268	1		
NDBI	0.122	0.080	−0.788 **	1	
NDVI	−0.088	−0.180	0.647 **	−0.939 **	1

\* Correlation is significant at the 0.05 level (two-tailed). \*\* Correlation is significant at the 0.01 level (two-tailed).

#### 4. Discussion

The findings of this study indicate that HAs characterised by high-density high-rise buildings experienced higher LST during the summer compared to HAs with less dense mid-rise and low-rise buildings. This observation was consistent with studies investigating the relationship between LST and urban morphology [35,86,87]. The importance of morphological features in HAs could not be underestimated, as they influenced the microclimate and ultimately contributed to a higher LST. The studied city parts are evaluated only for their morphological characteristics and LST, which are accepted to be not changeable for their geographical location, proximities, and closeness to each other.

The Space Syntax analysis, conducted to determine the impact of the street network integration index, one of the morphological indicators, on LST demonstrated remarkably high explanatory power on LST across all HAs exhibiting diverse morphological features. Nevertheless, it is noteworthy that the change in the correlation direction is based on the housing characteristics of each HA. We found a strong negative correlation between the integration index and LST in HA1 and HA3, similar to previous studies [30,31]. This indicates that integrated areas exhibit a more consistent cooling effect, showcasing stability in temperature regulation. However, it is noteworthy that the direction of the relationship between LST and the integration index varies depending on housing morphology. This relationship was notably reversed in HA2, which is dominated by high-rise, point block buildings, and we observed a significant positive correlation between the integration index and LST. It is also notable that the indicator has a cooling effect in low-rise and low-density areas, whereas it contributes to heating in high-rise and high-density areas. Point block buildings, a relatively new type compared to typical high-rise apartments, have rapidly developed since around 2010. The significant decrease in ventilation performance within closed forms of three or more buildings in point block developments may be a contributing factor. Moreover, due to the life cycle of densely populated and high-rise housing areas, greenhouse gas emissions are higher than in other areas [88]. Reduced ventilation not only contributes to an increase in air temperature but also contributes to an increase in surface temperature [59]. Therefore, the low ventilation performance in high-rise, high-density point block housing areas may have contributed to the increase in LST. These findings highlight the intricate relationship between urban design and temperature control and challenge previously conventional expectations. This study's results suggest that the effect of morphological features on microclimates varies between different housing areas, highlighting the need for tailored approaches to urban planning and design based on specific housing characteristics.

Drawing from the study's results, to effectively alleviate the UHI effect in low-rise housing areas, it is advisable, in alignment with prior research [30], to amplify the integration of urban spaces. This involves designing surfaces with higher integration that are more connected to the network [31] and constituting linear green street networks [30]. Conversely, in housing areas characterised by high-rise point blocks, it becomes pivotal to prioritise designs that curtail integration, thereby sustaining a lower LST environment. Recognising the detrimental impacts of greenhouse gas emissions on UHIs, it is imperative to promote the use of renewable energy sources such as solar and wind. Furthermore, the adoption of low-carbon emissions is paramount. In this context, the implementation of mechanisms, including carbon credits or caps, emerges as pragmatic and immediate solutions to curtail greenhouse gas emissions in the atmosphere [89].

NDBI and NDVI indices indicating land use intensity were positively correlated with NDBI and negatively correlated with NDVI in HA1 and HA2. The findings obtained are in light of the literature, and as Kikon et al. stated, likely due to the fact that vegetation and moisture-retaining soils use a relatively large fraction of the absorbed radiation in the process of evaporation (transpiration) and cool the surrounding air by releasing water vapour [89]. In harmony with prior research [35,74,90], NDBI demonstrated a positive correlation with LST in urban contexts. Notably, the study unveils a significant result: NDBI and NDVI indices were insufficient in explaining LST changes across housing areas in HA3. This limitation aligns with prior studies highlighting the constraints of NDBI and NDVI in elucidating LST [91,92]. It is worth noting that, despite previous studies emphasising the inability of these indices to capture LST in summer, this study, conducted during the same season, minimises the significance of the seasonal effect and demonstrates considerable potential in elucidating LST in HA1 and HA2. The study proposes two potential explanations for the underperformance of NDVI and NDBI indices in explaining LST in HA3. Firstly, the diversity of housing forms in the area, with irregular development and varying heights of houses, contrasts with the regular development of houses with similar heights in HA1 and HA2. This discrepancy may explain why NDBI is inadequate in elucidating LST in HA3, as its working principle, relying on building density, may not effectively compare NDBI values between unplanned, dense low-rise housing areas and 6- to 10-storey housing areas. Secondly, the higher spectral reflectance of bare soil in rural areas, especially in the SWIR band, compared to urban areas, is highlighted. Sparse and dry vegetation exhibits higher reflectance in the SWIR wavelength range compared to the NIR range, resulting in high NDBI values and low NDVI values in these areas. It is worth noting that the NDBI value of housing areas with a higher rural character in HA3 has a similarity with that of housing areas in the same region that have 6–10 storeys. Based on these findings, it could be speculated that NDBI and NDVI are inadequate in explaining LST in high-rural unplanned settlements such as HA3. The specific features of rural unplanned areas call for a specialised methodology to analyse the interplay of land use indicators and temperature trends. This highlights the importance of conducting more comprehensive studies to unveil the intricacies of the relationship between NDBI, NDVI, and LST in such environments.

In light of these results, it is imperative to initiate measures aimed at mitigating the UHI phenomenon, placing a primary emphasis on expanding the city's vegetation cover. The augmentation of greenery serves as a crucial factor in amplifying the rate of evapotranspiration [89]. Given the distinctive spatial configurations of planned and unplanned urban fabrics, it is recommended to prioritise the preservation of dense tree areas, elevate overall vegetation cover, and rehabilitate bare soil and bush lands with the integration of dense trees [30]. In the construction or transformation of urban blocks, it is crucial to consider not only the demands of urban development but also to prioritise the preservation of urban green spaces. Proactive planning of the urban green space system significantly contributes to enhancing cooling benefits, as evidenced by NDVI [93]. Strategic and thoughtful planning, including the intentional planting of trees, the incorporation of vegetation covers in urban areas, and the creation of green spaces, plays a pivotal role in cooling the atmosphere [94–96]. Implementing strategic measures, including planting trees

around housing areas, not only provides shade to urban surfaces, consequently reducing roof and wall temperatures, but also results in significant reductions in energy consumption for air conditioning [89]. Moreover, the shade generated by trees impedes the heating of enclosures and impermeable surfaces, contributing to the cooling rates of vegetated areas [42,97]. In conjunction with these strategies, the promotion of urban gardening, particularly the utilisation of private urban gardens such as vertical and rooftop gardens, emerges as an effective approach to mitigate the UHI effect. These measures contribute to the cooling of buildings and the conservation of energy consumption [98]. Furthermore, this practice also extends the lifespan of roofing materials compared to traditional rooftops, diminishes air pollutants and greenhouse gases, and enhances building insulation [89].

Following an analysis of the SVF to investigate the effect of housing form and height on surface temperature, we found a strong correlation between the SVF and LST in all HAs. This substantial characteristic of SVF aligns with previous reports [34,35,99]. There is a strong positive correlation between SVF and LST in low-density, low-rise, and mid-rise housing areas (HA1 and HA3). Areas with higher SVF values are known to receive more solar radiation and have higher temperatures compared to areas with lower SVF values [100,101]. Moreover, considering the morphological characteristics of HA3, it could be claimed that SVF is a better indicator than NDBI and NDVI in irregularly developed housing areas with high rural character, as a result of the positive correlation of SVF compared to NDBI and NDVI in explaining LST. However, in contrast to established knowledge, the direction of this correlation shifts within high-density housing area (HA2) that feature high-rise, point block buildings, similar to the analysis of the integration index. Notably, high-rise point block buildings, characterised by extreme SVF values (0.3), exhibit an elevation in LST. One possible reason is that the heat emitted from high-rise blocks could indeed be a contributing factor. An increased distance between the buildings improves airflow and allows the radiation to spread, while the ventilation level decreases in point blocks with low SVF [34,59]. Furthermore, while the courtyard and linear block buildings in the area have vegetation cover, point block buildings often have these areas covered with hard surfaces. In the courtyard and linear block buildings, the cooling effect of vegetation and the airflow around these buildings could lead to a decrease in LST. Therefore, in the HA2, there is a tendency for cooling in areas with high SVF, whereas in point block buildings with very low SVF, there is a tendency for heating. In light of these findings, it is evident that SVF proves to be a reliable indicator of LST in both planned and unplanned housing areas. However, contrary to initial expectations, the relationship between SVF and LST takes an unexpected turn in housing areas characterised by extremely low SVF values. In these areas, SVF serves as a negative indicator for LST, presenting a reversal of the anticipated correlation. This impressive result highlights the necessity for a more detailed understanding of the intricate interplay between SVF and LST, especially in areas characterised by extreme SVF values. Further research and in-depth investigations are crucial to unravelling the specific dynamics and contextual factors that contribute to this complex relationship, providing valuable insights for urban planning and environmental management in areas with extreme SVF conditions.

Considering the results of the study, as urban redevelopment progresses, the creation of diverse building heights and massing rather than a monolithic wall of high-rise buildings could effectively alleviate the UHI phenomenon [102–104]. To enhance the shielding effect of buildings and reduce the UHI effect of the city, it is recommended to replace worn textures with a well-balanced mix of compact mid-rises and open high-rises for new construction, thereby avoiding excessively high and extremely low SVF [35,59]. To counteract the UHI effect within the confined layouts of existing high-density high-rise buildings, it is suggested to integrate green spaces within the courtyards rather than employing impermeable surfaces [59].

## 5. Conclusions

Erzurum, one of the cities exposed to the largest amount of solar radiation in Turkey, has housing areas with different microclimate characteristics. In this paper, we comprehensively and objectively evaluated the 2D and 3D urban morphological indicators of housing areas and offered a framework to quantify the impact of urban morphology on microclimate.

The summer UHI effect within the high-rise buildings is severe, while the severity is relatively light in low-rise and mid-rise buildings; the impact of spatial form indicators on UHIs varies by HAs, with integrity index being the most correlated indicator with UHI in all HAs; some indicators have a more significant impact in specific HAs, such as SVF having a stronger impact on UHIs in HA2, where there is an extremely low SVF; the form, height, and arrangement of buildings are closely related to UHI; and the integrated distribution of mid-rise buildings is beneficial in reducing the UHI, while the segregated distribution of high-rise point blocks is effective in reducing the UHI. The reducing effect of NDVI on UHIs remains valid in the planned development of housing areas, with a larger proportion of vegetation in space showing a greater cooling effect on UHIs. Similarly, the enhancing effect of NDBI on UHIs remains valid in the planned development of housing areas with increased terrestrial radiation in the built-up area. On the contrary, land use intensity indices (NDBI, NDVI) are not good indicators for UHI studies in irregular housing areas with high rural character.

Drawing from the aforementioned research findings, our recommendation emphasises the importance of considering spatial and indicator-specific factors when optimising urban spatial forms to mitigate the UHI effect in urban design and spatial planning. It is essential to recognise that various indicators contribute differently to the urban heat environment in different HAs. As a result, developing strategies focused on specific indicators becomes imperative to effectively alleviate the UHI impact, taking into account the unique urban geometry characteristics of each HA. It is important to note that the UHI impact is closely associated with climate change. The warming climate will exacerbate already high temperatures in heat island areas. Therefore, the proposed mitigation and cooling strategies aimed at reducing UHIs could not only assist societies in adapting to the impacts of climate change but also contribute to the reduction in greenhouse gas emissions, which are a major cause of climate change.

This study's focus on summer surface temperature data limits the conclusions drawn about optimising urban heat environments to summer days. Moreover, the absence of winter data restricts the broader applicability of these findings. There is a need for deeper investigation into how morphological indicators impact UHI dynamics during winter, alongside the quest for pertinent solutions. This study, owing to its constrained scope and available data, leaves uncharted territory ripe for exploration. Exploring various vegetation types, assessing biomass, and delving into factors like rainfall, wind direction, speed, and various remote sensing indicators related to morphological structure (topographic position index, water index, and forest index) could substantially enrich our understanding of daily UHI fluctuations within urban morphology research. These unexplored elements hold the potential to illuminate critical nuances in how UHIs operates across different seasons and weather conditions.

**Author Contributions:** Conceptualization, C.G. and S.T.; methodology, C.G. and S.T.; formal analysis, C.G.; data curation, C.G. and S.T.; writing—original draft preparation, C.G. and S.T.; writing—review and editing, C.G. and S.T.; visualization, C.G. All authors have read and agreed to the published version of the manuscript.

**Funding:** This research received no external funding.

**Institutional Review Board Statement:** Not applicable.

**Informed Consent Statement:** Not applicable.

**Data Availability Statement:** Data are contained within the article.

**Conflicts of Interest:** The authors declare no conflicts of interest.

## References

- Kovats, R.S.; Campbell-Lendrum, D.; Matthies, F. Climate change and human health: Estimating avoidable deaths and disease. *Risk Anal.* **2005**, *25*, 1409–1418. [[CrossRef](#)] [[PubMed](#)]
- Song, J.; Chen, W.; Zhang, J.; Huang, K.; Hou, B.; Prishchepov, A.V. Effects of building density on land surface temperature in China: Spatial patterns and determinants. *Landsc. Urban Plan.* **2020**, *198*, 103794. [[CrossRef](#)]
- Wang, W.; Liu, K.; Tang, R.; Wang, S. Remote sensing image-based analysis of the urban heat island effect in Shenzhen, China. *Phys. Chem. Earth* **2019**, *110*, 168–175. [[CrossRef](#)]
- Li, J.; Song, C.; Cao, L.; Zhu, F.; Meng, X.; Wu, J. Impacts of landscape structure on surface urban heat islands: A case study of Shanghai, China. *Remote Sens. Environ.* **2011**, *115*, 3249–3263. [[CrossRef](#)]
- Wei, Y.D.; Ye, X. Urbanization, urban land expansion and environmental change in China. *Stoch. Environ. Res. Risk Assess.* **2014**, *28*, 757–765. [[CrossRef](#)]
- Zhou, L.; Yuan, B.; Hu, F.; Wei, C.; Dang, X.; Sun, D. Understanding the effects of 2D/3D urban morphology on land surface temperature based on local climate zones. *Build. Environ.* **2022**, *208*, 108578. [[CrossRef](#)]
- Zhu, Z.; Wang, G.; Dong, J. Correlation analysis between land use/cover change and air pollutants—A case study in Wuyishan city. *Energies* **2019**, *12*, 2545. [[CrossRef](#)]
- Srivastava, A.; Shukla, S.; Singh, P.; Jha, P.K. Spatio-temporal dynamics of land use/cover and land surface temperature in Prayagraj city, India. *Indoor Built Environ.* **2023**, *32*, 1250–1268. [[CrossRef](#)]
- Fikfak, A.; Kosanović, S.; Konjar, M.; Grom, J.P.; Zbašnik-Senegačnik, M. The impact of morphological features on summer temperature variations on the example of two residential neighborhoods in Ljubljana, Slovenia. *Sustainability* **2017**, *9*, 122. [[CrossRef](#)]
- Arbuthnott, K.G.; Hajat, S. The health effects of hotter summers and heat waves in the population of the United Kingdom: A review of the evidence. *Environ. Health* **2017**, *16*, 119. [[CrossRef](#)]
- Adeyemi, A.; Ramoelo, A.; Cho, M.A.; Strydom, J. Spatio-temporal analysis of built-up impervious surface area and interplay with land surface temperature in Pretoria, South Africa. *Geocarto Int.* **2022**, *37*, 7618–7638. [[CrossRef](#)]
- Çağlak, S. Investigation the relationship between causes of death and thermal comfort conditions: The sample of Amasya Province. *Int. J. Biometeorol.* **2023**, *67*, 1353–1362. [[CrossRef](#)] [[PubMed](#)]
- Cheval, S.; Dumitrescu, A.; Iraşoc, A.; Paraschiv, M.G.; Perry, M.; Ghent, D. MODIS-based climatology of the Surface Urban Heat Island at country scale (Romania). *Urban Clim.* **2022**, *41*, 101056. [[CrossRef](#)]
- Schlünzen, K.H.; Grimmond, S.; Baklanov, A. Development of the CL-UHI. In *Guidance to Measuring, Modelling and Monitoring the Canopy Layer Urban Heat Island*; WMO: Geneva, Switzerland, 2023; pp. 7–12. [[CrossRef](#)]
- Chew, L.W.; Norford, L.K. Pedestrian-level wind speed enhancement in urban street canyons with void decks. *Build. Environ.* **2018**, *146*, 64–76. [[CrossRef](#)]
- Hofman, J.; Castanheiro, A.; Nuyts, G.; Joosen, S.; Spassov, S.; Blust, R.; Wael, K.; Lenaerts, S.; Samson, R. Impact of urban street canyon architecture on local atmospheric pollutant levels and magneto-chemical PM10 composition: An experimental study in Antwerp, Belgium. *Sci. Total Environ.* **2020**, *712*, 135534. [[CrossRef](#)]
- Karimimoshaver, M.; Khalvandi, R.; Khalvandi, M. The effect of urban morphology on heat accumulation in urban street canyons and mitigation approach. *Sustain. Cities Soc.* **2021**, *73*, 103127. [[CrossRef](#)]
- Zhou, D.; Xiao, J.; Bonafoni, S.; Berger, C.; Deilami, K.; Zhou, Y.; Frolking, S.; Yao, R.; Qiao, Z.; Sobrino, J.A. Satellite remote sensing of surface urban heat islands: Progress, challenges, and perspectives. *Remote Sens.* **2018**, *11*, 48. [[CrossRef](#)]
- Zhou, X.; Chen, H. Impact of urbanization-related land use land cover changes and urban morphology changes on the urban heat island phenomenon. *Sci. Total Environ.* **2018**, *635*, 1467–1476. [[CrossRef](#)]
- He, B.J.; Ding, L.; Prasad, D. Relationships among local-scale urban morphology, urban ventilation, urban heat island and outdoor thermal comfort under sea breeze influence. *Sustain. Cities Soc.* **2020**, *60*, 102289. [[CrossRef](#)]
- Badaro-Saliba, N.; Adjizian-Gerard, J.; Zaarour, R.; Najjar, G. LCZ scheme for assessing Urban Heat Island intensity in a complex urban area (Beirut, Lebanon). *Urban Clim.* **2021**, *37*, 100846. [[CrossRef](#)]
- Hassan, T.; Zhang, J.; Prodhon, F.A.; Pangali Sharma, T.P.; Bashir, B. Surface urban heat islands dynamics in response to LULC and vegetation across South Asia (2000–2019). *Remote Sens.* **2021**, *13*, 3177. [[CrossRef](#)]
- Faisal, A.A.; Kafy, A.A.; Al Rakib, A.; Akter, K.S.; Jahir, D.M.A.; Sikdar, M.S.; Ashrafi, T.J.; Mallik, S.; Rahman, M.M. Assessing and predicting land use/land cover, land surface temperature and urban thermal field variance index using Landsat imagery for Dhaka Metropolitan area. *Environ. Chall.* **2021**, *4*, 100192. [[CrossRef](#)]
- Liu, X.; Ming, Y.; Liu, Y.; Yue, W.; Han, G. Influences of landform and urban form factors on urban heat island: Comparative case study between Chengdu and Chongqing. *Sci. Total Environ.* **2022**, *820*, 153395. [[CrossRef](#)] [[PubMed](#)]
- Allegrini, J.; Carmeliet, J. Simulations of local heat islands in Zürich with coupled CFD and building energy models. *Urban Clim.* **2018**, *24*, 340–359. [[CrossRef](#)]
- Guo, C.; Buccolieri, R.; Gao, Z. Characterizing the morphology of real street models and modelling its effect on thermal environment. *Energy Build.* **2019**, *203*, 109433. [[CrossRef](#)]

27. Liu, B.; Guo, X.; Jiang, J. How Urban Morphology Relates to the Urban Heat Island Effect: A Multi-Indicator Study. *Sustainability* **2023**, *15*, 10787. [[CrossRef](#)]
28. Seo, K.W.; Lee, S. Oxcart route in the city: Tracking the urbanization process of an agricultural village in Korea. *Sustainability* **2019**, *11*, 2153. [[CrossRef](#)]
29. Wang, X.; Yao, X.; Shao, H.; Bai, T.; Xu, Y.; Tian, G.; Fekete, A.; Kollányi, L. Land Use Quality Assessment and Exploration of the Driving Forces Based on Location: A Case Study in Luohe City, China. *Land* **2023**, *12*, 257. [[CrossRef](#)]
30. Nasehi, S.; Yavari, A.; Salehi, E.; Emmanuel, R. Role of local climate zone and space syntax on land surface temperature (case study: Tehran). *Urban Clim.* **2022**, *45*, 101245. [[CrossRef](#)]
31. Soltanifard, H.; Aliabadi, K. Impact of urban spatial configuration on land surface temperature and urban heat islands: A case study of Mashhad, Iran. *Theor. Appl. Climatol.* **2019**, *137*, 2889–2903. [[CrossRef](#)]
32. Hillier, B.; Turner, A.; Yang, T.; Park, H.T. Metric and topo-geometric properties of urban street networks: Some convergences, divergences and new results. In Proceedings of the 6th International Space Syntax Symposium 2007, Istanbul, Turkey, 12–15 June 2007; p. 22.
33. Scarano, M.; Sobrino, J.A. On the relationship between the sky view factor and the land surface temperature derived by Landsat-8 images in Bari, Italy. *Int. J. Remote Sens.* **2015**, *36*, 4820–4835. [[CrossRef](#)]
34. Hu, Y.; Dai, Z.; Guldmann, J.M. Modeling the impact of 2D/3D urban indicators on the urban heat island over different seasons: A boosted regression tree approach. *J. Environ. Manag.* **2020**, *266*, 110424. [[CrossRef](#)]
35. Zhu, Z.; Shen, Y.; Fu, W.; Zheng, D.; Huang, P.; Li, J.; Lan, Y.; Chen, Z.; Liu, A.; Xu, X.; et al. How does 2D and 3D of urban morphology affect the seasonal land surface temperature in Island City? A block-scale perspective. *Ecol. Indic.* **2023**, *150*, 110221. [[CrossRef](#)] [[PubMed](#)]
36. Susca, T.; Gaffin, S.R.; Dell’Osso, G.R. Positive effects of vegetation: Urban heat island and green roofs. *Environ. Pollut.* **2011**, *159*, 2119–2126. [[CrossRef](#)]
37. Li, X.; Zhou, W.; Ouyang, Z. Relationship between land surface temperature and spatial pattern of greenspace: What are the effects of spatial resolution? *Landsc. Urban Plan.* **2013**, *114*, 1–8. [[CrossRef](#)]
38. Feyisa, G.L.; Dons, K.; Meilby, H. Efficiency of parks in mitigating urban heat island effect: An example from Addis Ababa. *Landsc. Urban Plan.* **2014**, *123*, 87–95. [[CrossRef](#)]
39. Dos Santos, A.R.; de Oliveira, F.S.; da Silva, A.G.; Gleriani, J.M.; Gonçalves, W.; Moreira, G.L.; Silva, F.G.; Branco, E.R.F.; Moura, M.M.; da Silva, R.G.; et al. Spatial and temporal distribution of urban heat islands. *Sci. Total Environ.* **2017**, *605*, 946–956. [[CrossRef](#)]
40. Karakuş, C.B. The impact of land use/land cover (LULC) changes on land surface temperature in Sivas City Center and its surroundings and assessment of Urban Heat Island. *Asia-Pac. J. Atmos. Sci.* **2019**, *55*, 669–684. [[CrossRef](#)]
41. Hua, L.; Zhang, X.; Nie, Q.; Sun, F.; Tang, L. The impacts of the expansion of urban impervious surfaces on urban heat islands in a coastal city in China. *Sustainability* **2020**, *12*, 475. [[CrossRef](#)]
42. Yang, C.; Yan, F.; Zhang, S. Comparison of land surface and air temperatures for quantifying summer and winter urban heat island in a snow climate city. *J. Environ. Manag.* **2020**, *265*, 110563. [[CrossRef](#)]
43. Pakarnsee, R.; Chunkao, K.; Bualert, S. Physical characteristics of Bangkok and its urban heat island phenomenon. *Build Environ.* **2018**, *143*, 561–569. [[CrossRef](#)]
44. He, T.; Zhou, R.; Ma, Q.; Li, C.; Liu, D.; Fang, X.; Yina, H.; Gao, J. Quantifying the effects of urban development intensity on the surface urban heat island across building climate zones. *Appl. Geogr.* **2023**, *158*, 103052. [[CrossRef](#)]
45. Sun, F.; Liu, M.; Wang, Y.; Wang, H.; Che, Y. The effects of 3D architectural patterns on the urban surface temperature at a neighborhood scale: Relative contributions and marginal effects. *J. Clean. Prod.* **2020**, *258*, 120706. [[CrossRef](#)]
46. Peng, S.; Piao, S.; Ciais, P.; Friedlingstein, P.; Otle, C.; Bréon, F.M.; Nan, H.; Zhou, L.; Myneni, R.B. Surface urban heat island across 419 global big cities. *Environ. Sci. Technol.* **2012**, *46*, 696–703. [[CrossRef](#)]
47. Clinton, N.; Gong, P. MODIS detected surface urban heat islands and sinks: Global locations and controls. *Remote Sens. Environ.* **2013**, *134*, 294–304. [[CrossRef](#)]
48. Li, X.; Zhou, Y.; Asrar, G.R.; Imhoff, M.; Li, X. The surface urban heat island response to urban expansion: A panel analysis for the conterminous United States. *Sci. Total Environ.* **2017**, *605*, 426–435. [[CrossRef](#)]
49. Dai, Z.; Guldmann, J.M.; Hu, Y. Spatial regression models of park and land-use impacts on the urban heat island in central Beijing. *Sci. Total Environ.* **2018**, *626*, 1136–1147. [[CrossRef](#)] [[PubMed](#)]
50. Huang, Q.; Lu, Y. Urban heat island research from 1991 to 2015: A bibliometric analysis. *Theor. Appl. Climatol.* **2018**, *131*, 1055–1067. [[CrossRef](#)]
51. Dursun, D.; Güller, C. Relationship between child and urban space: Accessibility and areal efficiency analysis of playgrounds in Erzurum. *J. Grad. Sch. Nat. Appl. Sci. Mehmet Akif Ersoy Univ.* **2019**, *10*, 11–27. [[CrossRef](#)]
52. Available online: <https://atlas.harita.gov.tr> (accessed on 1 December 2023).
53. Lee, J.; Lee, Y.G.; Kim, B.J. Analysis of the thermal environment around an urban green area in Seoul, Korea using Climate Analysis Seoul (CAS). *Atmosphere* **2016**, *26*, 413–421. [[CrossRef](#)]
54. Park, J.H.; Cho, G.H. Examining the association between physical characteristics of green space and land surface temperature: A case study of Ulsan, Korea. *Sustainability* **2016**, *8*, 777. [[CrossRef](#)]

55. Srivani, M.; Kazunori, H. The influence of urban morphology indicators on summer diurnal range of urban climate in Bangkok metropolitan area, Thailand. *Int. J. Civ. Environ. Eng.* **2011**, *11*, 34–46.
56. Lee, K.; Kim, Y.; Sung, H.C.; Kim, S.H.; Jeon, S.W. Surface urban heat island in South Korea's new towns with different urban planning. *E Environ. Monit. Assess.* **2022**, *194*, 360. [[CrossRef](#)] [[PubMed](#)]
57. Thanvisitthpon, N. Statistically Validated Urban Heat Island Risk Indicators for UHI Susceptibility Assessment. *Int. J. Environ. Res. Public Health* **2023**, *20*, 1172. [[CrossRef](#)] [[PubMed](#)]
58. Yu, X.; Guo, X.; Wu, Z. Land surface temperature retrieval from Landsat 8 TIRS—Comparison between radiative transfer equation-based method, split window algorithm and single channel method. *Remote Sens.* **2014**, *6*, 9829–9852. [[CrossRef](#)]
59. Kim, J.; Lee, D.K.; Brown, R.D.; Kim, S.; Kim, J.H.; Sung, S. The effect of extremely low sky view factor on land surface temperatures in urban residential areas. *Sustain. Cities Soc.* **2022**, *80*, 103799. [[CrossRef](#)]
60. Liu, J.; Feng, Q.; Gong, J.; Zhou, J.; Liang, J.; Li, Y. Winter wheat mapping using a random forest classifier combined with multi-temporal and multi-sensor data. *Int. J. Digit. Earth* **2018**, *11*, 783–802. [[CrossRef](#)]
61. Nadizadeh Shorabeh, S.; Hamzeh, S.; Zanganeh Shahraki, S.; Firozjaei, M.K.; Jokar Arsanjani, J. Modelling the intensity of surface urban heat island and predicting the emerging patterns: Landsat multi-temporal images and Tehran as case study. *Int. J. Remote Sens.* **2020**, *41*, 7400–7426. [[CrossRef](#)]
62. Hillier, B. Space is the machine: A configurational theory of architecture. *J. Urban Des.* **2007**, *3*, 333–335.
63. Liu, X.; Jiang, B. Defining and generating axial lines from street center lines for better understanding of urban morphologies. *Int. J. Geogr. Inf. Syst.* **2012**, *26*, 1521–1532. [[CrossRef](#)]
64. Johnsson, C.; Camporeale, R. Exploring Space Syntax Integration at Public Transport Hubs and Public Squares Using Drone Footage. *Appl. Sci.* **2022**, *12*, 6515. [[CrossRef](#)]
65. Crucitti, P.; Latora, V.; Porta, S. Centrality in networks of urban streets. *Chaos* **2006**, *16*, 015113. [[CrossRef](#)] [[PubMed](#)]
66. Xia, C.; Zhang, A.; Wang, H.; Yeh, A.G. Predicting the expansion of urban boundary using space syntax and multivariate regression model. *Habitat Int.* **2019**, *86*, 126–134. [[CrossRef](#)]
67. Chapman, L.; Thornes, J.E. Real-time sky-view factor calculation and approximation. *J. Atmos. Ocean. Technol.* **2004**, *21*, 730–741. [[CrossRef](#)]
68. Grimmond, C.S.B.; Potter, S.K.; Zutter, H.N.; Souch, C. Rapid methods to estimate sky-view factors applied to urban areas. *Int. J. Climatol.* **2001**, *21*, 903–913. [[CrossRef](#)]
69. Shaker, R.R.; Drezner, T.D. A New Technique for Predicting the Sky-View Factor for Urban Heat Island Assessment. *Geogr. Bull.* **2010**, *51*, 85–96.
70. Svensson, M.K. Sky view factor analysis—implications for urban air temperature differences. *Meteorol. Appl.* **2004**, *11*, 201–211. [[CrossRef](#)]
71. Debbage, N. Sky-view factor estimation: A case study of Athens, Georgia. *Geogr. Bull.* **2013**, *54*, 49.
72. Halder, B.; Bandyopadhyay, J.; Banik, P. Monitoring the effect of urban development on urban heat island based on remote sensing and geo-spatial approach in Kolkata and adjacent areas, India. *Sustain. Cities Soc.* **2021**, *74*, 103186. [[CrossRef](#)]
73. Hidalgo-García, D.; Arco-Díaz, J. Modeling the Surface Urban Heat Island (SUHI) to study of its relationship with variations in the thermal field and with the indices of land use in the metropolitan area of Granada (Spain). *Sustain. Cities Soc.* **2022**, *87*, 104166. [[CrossRef](#)]
74. Mansour, K.; Aziz, M.A.; Hashim, S.; Effat, H. Impact of anthropogenic activities on urban heat islands in major cities of El-Minya Governorate, Egypt. *Egypt. J. Remote Sens. Space Sci.* **2022**, *25*, 609–620. [[CrossRef](#)]
75. Kshetri, T. Ndvi, ndbi & ndwi calculation using landsat 7, 8. *GeoWorld* **2018**, *2*, 32–34.
76. Wang, J.; Rich, P.M.; Price, K.P. Temporal responses of NDVI to precipitation and temperature in the central Great Plains, USA. *Int. J. Remote Sens.* **2003**, *24*, 2345–2364. [[CrossRef](#)]
77. Pettorelli, N.; Vik, J.O.; Mysterud, A.; Gaillard, J.M.; Tucker, C.J.; Stenseth, N.C. Using the satellite-derived NDVI to assess ecological responses to environmental change. *Trends Ecol. Evol.* **2005**, *20*, 503–510. [[CrossRef](#)]
78. Huang, S.; Tang, L.; Hupy, J.P.; Wang, Y.; Shao, G. A commentary review on the use of normalized difference vegetation index (NDVI) in the era of popular remote sensing. *J. For. Res.* **2021**, *32*, 1–6. [[CrossRef](#)]
79. Li, S.; Xu, L.; Jing, Y.; Yin, H.; Li, X.; Guan, X. High-quality vegetation index product generation: A review of NDVI time series reconstruction techniques. *Int. J. Appl. Earth Obs. Geoinf.* **2021**, *105*, 102640. [[CrossRef](#)]
80. Zha, Y.; Gao, J.; Ni, S. Use of normalized difference built-up index in automatically mapping urban areas from TM imagery. *Int. J. Remote Sens.* **2003**, *24*, 583–594. [[CrossRef](#)]
81. He, C.; Shi, P.; Xie, D.; Zhao, Y. Improving the normalized difference built-up index to map urban built-up areas using a semiautomatic segmentation approach. *Remote Sens. Lett.* **2010**, *1*, 213–221. [[CrossRef](#)]
82. Gál, T.; Lindberg, F.; Unger, J. Computing continuous sky view factors using 3D urban raster and vector databases: Comparison and application to urban climate. *Theor. Appl. Climatol.* **2009**, *95*, 111–123. [[CrossRef](#)]
83. Cai, Z.; Han, G.; Chen, M. Do water bodies play an important role in the relationship between urban form and land surface temperature? *Sustain. Cities Soc.* **2018**, *39*, 487–498. [[CrossRef](#)]
84. Syafitri, R.A.; Pamungkas, A.; Santoso, E.B. Urban form factors that play important roles on UHI spatial-temporal pattern: A case study of East Surabaya, Indonesia. In Proceedings of the IOP Conference Series: Earth and Environmental Science (ICIAP 2020), Universitas Gadjah Mada, Yogyakarta, Indonesia, 15–16 October 2020; pp. 764–773.

85. Anselin, L. Local indicators of spatial association-LISA. *Geogr. Anal.* **1995**, *27*, 93–115. [[CrossRef](#)]
86. Adulkongkaew, T.; Satapanajaru, T.; Charoenhirunyingsos, S.; Singhirunnusorn, W. Effect of land cover composition and building configuration on land surface temperature in an urban-sprawl city, case study in Bangkok Metropolitan Area, Thailand. *Heliyon* **2020**, *6*, e04485. [[CrossRef](#)]
87. Ghosh, S.; Kumar, D.; Kumari, R. Assessing spatiotemporal dynamics of land surface temperature and satellite-derived indices for new town development and suburbanization planning. *Urban Gov.* **2022**, *2*, 144–156. [[CrossRef](#)]
88. Pomponi, F.; Saint, R.; Arehart, J.H.; Gharavi, N.; D’Amico, B. Decoupling density from tallness in analysing the life cycle greenhouse gas emissions of cities. *NPJ Urban Sustain.* **2021**, *1*, 33. [[CrossRef](#)]
89. Kikon, N.; Singh, P.; Singh, S.K.; Vyas, A. Assessment of urban heat islands (UHI) of Noida City, India using multi-temporal satellite data. *Sustain. Cities Soc.* **2016**, *22*, 19–28. [[CrossRef](#)]
90. Aslam, A.; Rana, I.A.; Bhatti, S.S. The spatiotemporal dynamics of urbanisation and local climate: A case study of Islamabad, Pakistan. *Environ. Impact Assess. Rev.* **2021**, *91*, 106666. [[CrossRef](#)]
91. Chen, L.; Li, M.; Huang, F.; Xu, S. Relationships of LST to NDBI and NDVI in Wuhan City based on Landsat ETM+ image. *CISP* **2013**, *2*, 840–845. [[CrossRef](#)]
92. Mathew, A.; Khandelwal, S.; Kaul, N. Investigating spatial and seasonal variations of urban heat island effect over Jaipur city and its relationship with vegetation, urbanization and elevation parameters. *Sustain. Cities Soc.* **2017**, *35*, 157–177. [[CrossRef](#)]
93. Yao, X.; Zhu, Z.; Zeng, X.; Huang, S.; Liu, Q.; Yu, K.; Zhou, X.; Chen, Z.; Liu, J. Linking maximum-impact and cumulative-impact indices to quantify the cooling effect of waterbodies in a subtropical city: A seasonal perspective. *Sustain. Cities Soc.* **2022**, *82*, 103902. [[CrossRef](#)]
94. Lin, W.; Yu, T.; Chang, X.; Wu, W.; Zhang, Y. Calculating cooling extents of green parks using remote sensing: Method and test. *Landsc. Urban Plan.* **2015**, *134*, 66–75. [[CrossRef](#)]
95. Tan, K.; Liao, Z.; Du, P.; Wu, L. Land surface temperature retrieval from Landsat 8 data and validation with geosensor network. *Front. Earth Sci.* **2017**, *11*, 20–34. [[CrossRef](#)]
96. Aram, F.; García, E.H.; Solgi, E.; Mansournia, S. Urban green space cooling effect in cities. *Heliyon* **2019**, *5*, 01339. [[CrossRef](#)]
97. Li, T.; Meng, Q. A mixture emissivity analysis method for urban land surface temperature retrieval from Landsat 8 data. *Landsc. Urban Plan.* **2018**, *179*, 63–71. [[CrossRef](#)]
98. Humaida, N.; Saputra, M.H.; Hadiyan, Y. Urban gardening for mitigating heat island effect. *IOP Conf. Ser. Earth Environ. Sci.* **2022**, *1133*, 012048. [[CrossRef](#)]
99. Chen, Q.; Cheng, Q.; Chen, Y.; Li, K.; Wang, D.; Cao, S. The Influence of Sky View Factor on Daytime and Nighttime Urban Land Surface Temperature in Different Spatial-Temporal Scales: A Case Study of Beijing. *Remote Sens.* **2021**, *13*, 4117. [[CrossRef](#)]
100. Scarano, M.; Mancini, F. Assessing the relationship between sky view factor and land surface temperature to the spatial resolution. *Int. J. Remote Sens.* **2017**, *38*, 6910–6929. [[CrossRef](#)]
101. Taripanah, F.; Ranjbar, A. Quantitative analysis of spatial distribution of land surface temperature (LST) in relation Ecohydrological, terrain and socio-economic factors based on Landsat data in mountainous area. *Adv. Space Res.* **2021**, *68*, 3622–3640. [[CrossRef](#)]
102. Taslim, S.; Parapari, D.M.; Shafaghat, A. Urban design guidelines to mitigate urban heat island (UHI) effects in hot-dry cities. *J. Teknol.* **2015**, *74*, 119–124. [[CrossRef](#)]
103. Bechtel, B.; Daneke, C. Classification of local climate zones based on multiple earth observation data. *IEEE J. Sel. Top. Appl. Earth Obs. Remote Sens.* **2012**, *5*, 1191–1202. [[CrossRef](#)]
104. Kaloustian, N.; Bechtel, B. Local climatic zoning and urban heat island in Beirut. *Procedia Eng.* **2016**, *169*, 216–223. [[CrossRef](#)]

**Disclaimer/Publisher’s Note:** The statements, opinions and data contained in all publications are solely those of the individual author(s) and contributor(s) and not of MDPI and/or the editor(s). MDPI and/or the editor(s) disclaim responsibility for any injury to people or property resulting from any ideas, methods, instructions or products referred to in the content.